Superhard BC$_3$ in Cubic Diamond Structure

Miao Zhang,[1,2] Hanyu Liu,[1] Quan Li,[3,1,*] Bo Gao,[1] Yanchao Wang,[1] Hongdong Li,[1]
Changfeng Chen,[4,†] and Yanming Ma[1,‡]

[1]*State Key Laboratory of Superhard Materials, Jilin University, Changchun 130012, China*
[2]*College of Physics, Beihua University, Jilin 132013, China*
[3]*College of Materials Science and Engineering, Jilin University, Changchun 130012, China*
[4]*Department of Physics and High Pressure Science and Engineering Center, University of Nevada,
Las Vegas, Nevada 89154, USA*

We solve the crystal structure of recently synthesized cubic BC$_3$ using an unbiased swarm structure search, which identifies a highly symmetric BC$_3$ phase in the cubic diamond structure (d-BC$_3$) that contains a distinct B-B bonding network along the body diagonals of a large 64-atom unit cell. Simulated x-ray diffraction and Raman peaks of d-BC$_3$ are in excellent agreement with experimental data. Calculated stress-strain relations of d-BC$_3$ demonstrate its intrinsic superhard nature and reveal intriguing sequential bond-breaking modes that produce superior ductility and extended elasticity, which are unique among superhard solids. The present results establish the first boron carbide in the cubic diamond structure with remarkable properties, and these new findings also provide insights for exploring other covalent solids with complex bonding configurations.

Diamond is the best known superhard material, but its utility is limited by several shortcomings, including brittleness, a tendency to react with iron, and oxidization in air at high temperature. Exploration of other strong covalent materials in the cubic diamond structure has produced considerable success, and the most famous example is cubic boron nitride (c-BN), which exhibits significantly improved stability against oxidation and reaction with ferrous metals. Efforts also have been directed toward improving the ductility and stability of diamond through boron doping [1–3]. Boron doped diamond turns into a hole-doping metal and even a superconductor when the dopant concentration is higher than 2% [4]. These intriguing properties have stimulated great interest in searching for boron carbides in the diamond structure with a high boron content.

Boron incorporation into the diamond lattice has been notoriously hard since the resulting B-C phases are often unstable. Use of precursor materials, such as graphitelike B-C phases synthesized by chemical vapor deposition, is a common approach to growing diamondlike B-C phases through phase transformations at high pressure and high temperature conditions. During such transformations, two-dimensional graphitic sp^2 bonding converts into three-dimensional sp^3 bonding. Using this approach, Solozhenko *et al.* synthesized a diamondlike superhard BC$_5$ phase (c-BC$_5$) at 24 GPa and 2200 K [5]. Most recently, a new cubic BC$_3$ (c-BC$_3$) phase was synthesized by direct transformation of graphitic BC$_3$ at 39 GPa and 2200 K [6]. Electron energy loss spectroscopy measurements show that this c-BC$_3$ is a single phase with all the atoms forming an sp^3 bonding network. Several structural models have been

proposed for c-BC$_5$ and c-BC$_3$ [7–12]; however, they all suffer from incorrect crystal symmetry and even the wrong bonding character compared to the experimentally observed diamondlike cubic structure with all the atoms in the sp^3 bonding state. This lack of an accurate structural determination impedes further understanding and exploration of these novel B-C compounds, and it calls for an innovative approach to solving such complex crystal structures. Of particular interest here is the distribution of boron atoms and their bonding network in the diamond lattice and its role in stabilizing the structure and influencing physical properties.

In this Letter, we report the structural determination of the newly synthesized c-BC$_3$ using an unbiased swarm structure search. Our work identifies a BC$_3$ phase in the cubic diamond structure, which contains a distinct boron bonding network along the body diagonals of its 64-atom unit cell. This new structure conforms to the experimental constraints on the cubic crystal symmetry and all-sp^3 bonding type, and its simulated x-ray diffraction and Raman spectra almost perfectly match the experimental data. The highly symmetric boron bonding network plays an important role in stabilizing the cubic diamond structure. Calculated stress-strain relations reveal its intrinsic superhard nature combined with superior ductility driven by intriguing sequential bond-breaking processes that do not exist in diamond or c-BN. These results establish the first cubic diamond phase in boron carbides and unveil its remarkable structural properties. This work serves as an exemplary case study of strong covalent solids with complex bonding configurations, and the insights gained

here may help explore other complex binary and ternary covalent compounds.

For the structure search we employed the swarm-intelligence based CALYPSO method and its same name code [13,14], which was unbiased by any prior known structures. The approach has correctly predicted the crystal structures of a diverse variety of materials [15–17]. *Ab initio* structural relaxation and electronic band-structure calculations were carried out using density functional theory with the Perdew-Burke-Ernzerh generalized gradient approximation [18] exchange-correlation potential as implemented in the VASP code [19]. The all-electron projector-augmented wave method [20] was adopted with the choice of $1s^2$ cores for both boron and carbon atoms. An energy cutoff of 800 eV for the plane-wave expansion and a Monkhorst-Pack k-point mesh of $8 \times 8 \times 8$ in the Brillouin zone produced enthalpy results well converged to below 1 meV/f.u. The lattice dynamics calculations used both the direct supercell method [21,22] and linear response theory [23]. Raman peak calculations were carried out using density functional perturbation theory as implemented in the QUANTUM-ESPRESSO code [23] with an energy cutoff of 80 Ry.

To search for BC_3 structures in sp^3 bonding we used simulation cells up to 16 formula units (64 atoms/cell) in the pressure range of 0–100 GPa, and our simulations reproduced previously proposed BC_3 structures in orthorhombic *Pmma-a* [8], *Pmma-b* [8], and tetragonal *P-4m2* [7] symmetry, which are all different from the experimentally determined cubic symmetry. Our unbiased structural search successfully identified a previously unknown BC_3 phase in the highly symmetric cubic diamond structure (denoted as d-BC_3, space group I-$43m$, 64 atoms/cell). This structure, shown in Fig. 1, is in stark contrast to the previously proposed BC_3 phases that all contain a boron layer between carbon layers, causing a large distortion of the diamond lattice. The cubic d-BC_3 structure, however, does not have a layered boron structure; instead, it can be built as a $2 \times 2 \times 2$ supercell of the cubic diamond structure with boron atoms substituting carbon atoms along the body-diagonal directions, forming a distinct B-B bonding network in the diamond lattice. This distribution of B-B bonds in the cubic cell enables the maintaining of the diamond lattice and helps
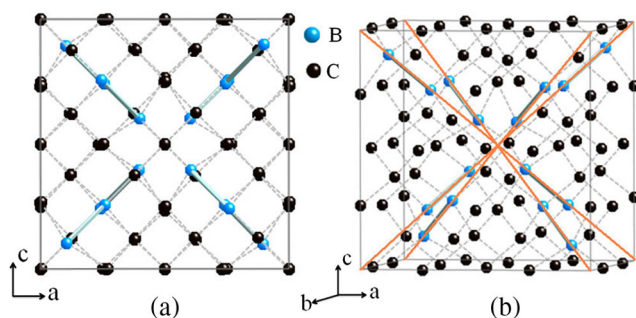
its dense packing and stability. At ambient pressure, the optimized lattice parameter of d-BC_3 is $a = 7.330$ Å, with boron occupying $8c$ (0.89711,0.89711,0.10289) and $8c$ (0.24273,0.24273,0.75727), and carbon occupying $12e$ (0.26755,0.0,0.0), $12d$ (0.0,0.5,0.75) and $24g$ (0.61792, 0.87580,0.87580). This arrangement of boron atoms in the diamond lattice in d-BC_3 provides useful insights for modeling other BC_x and even more complex ternary B-C-N systems. We have calculated the elastic constants of d-BC_3 and obtained $C_{11} = 658.4$ GPa, $C_{44} = 392.5$ GPa, and $C_{12} = 194.7$ GPa, which satisfy the mechanical stability criteria for a cubic crystal, i.e., $C_{44} > 0$, $C_{11} > C_{12}$, and $C_{11} + 2C_{12} > 0$. We also calculated the Vickers hardness using a semiempirical model [24,25] and obtained 62 GPa, which places d-BC_3 well above the threshold (40 GPa) for a superhard material and puts it close to c-BN (72 GPa) in hardness.

A Bader charge analysis reveals that the charge density at the B-B bond critical point is 0.463 electrons/Å^3 with a Laplacian value of -1.14, indicating the covalent nature of the B-B bond in d-BC_3. The calculated enthalpy shows that d-BC_3 becomes the most stable BC_3 structure with exclusively sp^3 hybridization bonding above 41.3 GPa [Fig. 2(a)], in good agreement with the experimental synthesis pressure of 39 GPa [6]. Also shown in Fig. 2(a) is the enthalpy of a recently proposed $R3m$ structure [12], which is energetically more favorable than all the predicted sp^3 bonded structures. However, this $R3m$ structure contains a mixture of sp^2 and sp^3 bonding, which is in contrast to the exclusively sp^3 bonding nature of the synthesized diamondlike BC_3 [6]. The calculated electronic density of states [Fig. 2(b)] shows substantial overlap of the C-p and B-p states, indicating strong covalent B-C bonding in d-BC_3. The absence of imaginary frequency modes in the Brillouin zone [Fig. 2(c)] confirms the dynamical stability of d-BC_3. The calculated electronic band structure of d-BC_3 at equilibrium shows that

FIG. 1 (color online). Predicted d-BC_3 structure. (a) A view along one of the cubic axes and (b) a polyhedral view.
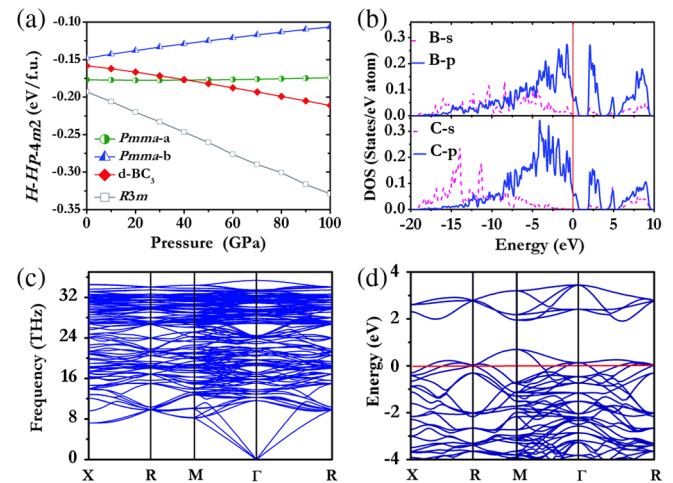

FIG. 2 (color online). (a) Calculated enthalpy versus pressure for various BC_3 structures relative to that of the P-$4m2$ phase. (b)–(d) Calculated electronic density of states, phonon dispersion, and electronic band structure of d-BC_3 at 0 GPa.

the top of its bonding state is 0.7 eV above the Fermi level [Fig. 2(d)], suggesting a hole-conducting behavior.

We have simulated x-ray diffraction (XRD) patterns of the d-BC$_3$ structure and compared the results with the experimental XRD data [Fig. 3(a)]. The four main peaks of d-BC$_3$ at a d spacing of 0.889, 1.083, 1.269, and 2.075 Å match the experimental data almost perfectly. Meanwhile, the simulated XRD patterns of the $R3m$ structure do not match the experimental XRD data (see the Supplemental Material [26] for details), ruling out the $R3m$ structure as the candidate of experimental diamondlike BC$_3$. The metallic nature of d-BC$_3$ precludes a direct Raman intensity calculation within the well-documented polarization method [44]. It is, however, still possible to determine the zone-center phonon modes and compare the calculated results with the experimental Raman data. Results in Fig. 3(b) show that the calculated Raman peaks of d-BC$_3$ provide a good description of the experimental Raman spectrum [6], giving additional support to the structural assignment of the d-BC$_3$ phase for the experimentally synthesized c-BC$_3$.

Boron and carbon have similar atomic radii, making site disorder a possibility in boron carbides [5,12]. We have simulated disordered BC$_3$ alloys using a special quasirandom structure model [45,46] for the distribution of boron and carbon atoms in fully relaxed diamond-lattice-based n-atom (n = 16, 32, 64, and 128) supercells [26]. The calculations show that the ordered d-BC$_3$ structure is energetically more favorable than the disordered structures in the pressure range of 0–40 GPa at $T = 0$ K. We also calculated the Gibbs free energy including the vibrational and configurational entropy contributions using a 128-atom supercell, and the results show that the d-BC$_3$ structure has lower Gibbs free energy than that of the quasirandom structure up to 1166 K [26]. Since the diamondlike BC$_3$ phase was obtained by quenching the sample from the synthesizing temperature (2200 K) to ambient temperature, this result suggests a temperature-induced disorder-order transition and further supports the predicted d-BC$_3$ structure.

We now examine the fundamental structural and mechanical properties of d-BC$_3$. We performed first-principles calculations of the stress-strain relations, which provide insights into the local bond deformation and breaking mechanisms that determine the incipient plasticity in a crystal [47]. We assess the stress response under tensile and shear strains to establish the respective ideal strength, i.e., the lowest stress to plastically deform a perfect crystal, which sets an upper bound for material strength that can be reached in high-quality samples [48]. Such calculations have been extensively applied to strong solids under a variety of loading conditions [49–54]. Here, we follow the established method and first determine the stress-strain relation for d-BC$_3$ under tensile strains in three principal symmetry crystallographic directions.

The calculated peak stresses (Fig. 4) are 107.6, 77.6, and 52.5 GPa in the ⟨100⟩, ⟨110⟩, and ⟨111⟩ directions, respectively, which indicate that the body diagonal ⟨111⟩ is the weakest tensile direction, and thus the (111) planes are the easy cleavage planes. This result is consistent with the body-diagonal alignment of the weak B-B bonds. Results on bond lengths under the ⟨111⟩ strain (Fig. 4) clearly show that, while the B-B bond continues to weaken at increasing strain, the peak tensile stress (i.e., the ideal
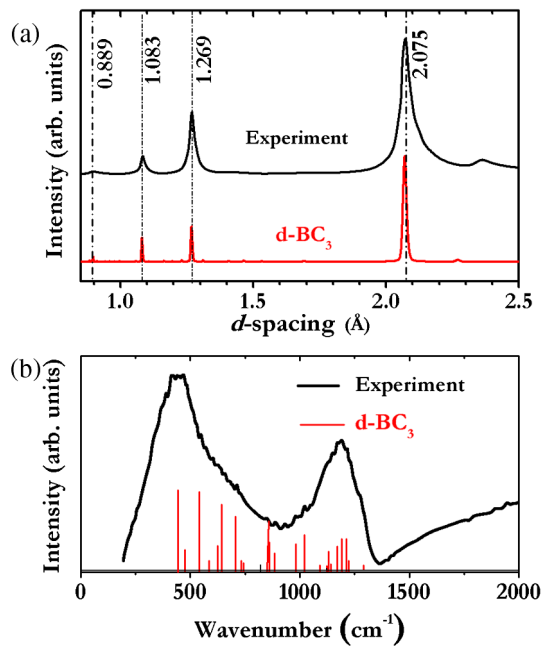

FIG. 3 (color online). (a) Simulated XRD of d-BC$_3$ compared to experimental data [6]. The x-ray wavelength is 0.3681 Å in both cases. (b) Simulated Raman peaks of d-BC$_3$ compared to the experimental Raman spectrum at ambient pressure.
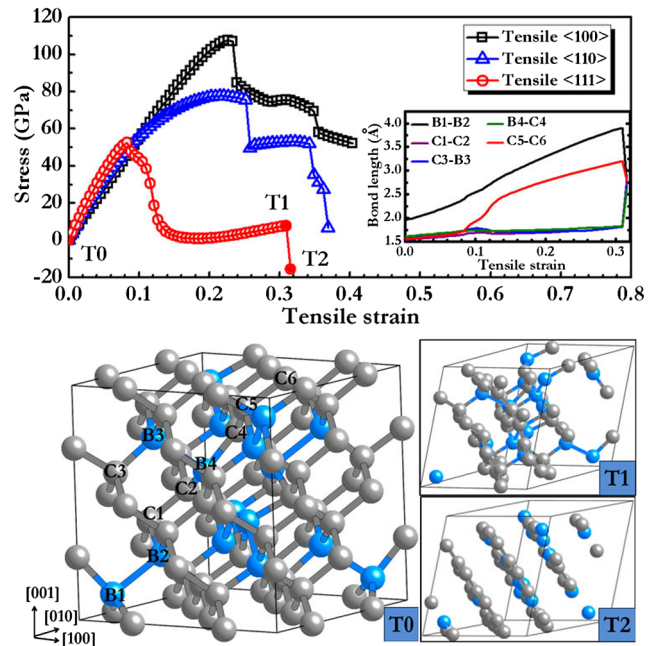

FIG. 4 (color online). Top panel: calculated tensile stress-strain relations for d-BC$_3$. Inset shows bond lengths under the ⟨111⟩ strain. Bottom panels: structural snapshots corresponding to the filled symbols in the stress-strain plot.

tensile strength) of d-BC_3 coincides with the onset of a sudden increase of elongation of the C5-C6 carbon bonds at the tensile strain of 0.08. It indicates that these C-C bonds are the main load bearing component, but the overall strength of d-BC_3 is lower compared to diamond because of the reduced density of C-C bonds, which have been partially replaced by B-C and B-B bonds in the $\langle 111 \rangle$ direction. Interestingly, the $\langle 111 \rangle$ tensile stress decreases very gradually past the peak and the peak-to-valley drop extends over a wide range of tensile strain from 0.08 to 0.18. This behavior is highly unusual for a superhard material, and it is in stark contrast to the results for diamond and c-BN where the stress drops precipitously past the peak [49–51]. Even more striking, the system undergoes a second elastic response regime from tensile strain 0.18 to 0.31 with the stress rising to 7.7 GPa (at $T1$) before its final graphitization ($T2$). This surprising ductility and extended elastic behavior of d-BC_3 stems from the modulation of the bonding environment by boron in the diamond lattice. Right past the tensile stress peak, the gradual stress decrease ensues because the stronger C-C bonds have been partially substituted by the softer B-C and B-B bonds along the $\langle 111 \rangle$ direction. After the stress release by the breaking of the C-C bonds, the B-C bonds become the main load bearing component, producing the second elastic response regime. All this can be attributed to the unique sequential bond-breaking process in d-BC_3, which contains multiple types of bonds with different strengths and different breaking strains, in sharp contrast to diamond and c-BN, which each comprise only one type of bond that breaks simultaneously at the peak strain with an immediate steep drop of stress.

We next evaluate the shear stress response in the (111) easy cleavage plane of d-BC_3. The stress peaks are nearly isotropic along different shear directions (Fig. 5), which is in contrast to the results of diamond and c-BN, which exhibit a large anisotropy in peak shear stress of about 40% in the easy cleavage plane [51]. Moreover, the lowest peak shear stress (i.e., the ideal shear strength) of 53.0 GPa in the $(111)[0\bar{1}1]$ shear direction is almost identical to the ideal tensile strength (52.5 GPa). These strength values place d-BC_3 as a superhard material close to c-BN [51], and the ratio of near unity for shear over tensile strength (53.0/52.5) is the lowest among superhard covalent materials [50], indicating the superior ductility of d-BC_3 among top superhard materials. Here, the ideal shear strength is limited by the sequential breaking of the B-C and then B-B bonds, followed by additional B-C and C-C bond breaking (see the inset in Fig. 5). Similar sequential bonding breaking processes also occur under the shear deformation along the $(111)[\bar{1}\,\bar{1}\,2]$ and $(111)[11\bar{2}]$ directions, which reduce the peak stresses and produce the nearly isotropic shear stress response in the (111) plane of d-BC_3. These fascinating tensile and shear stress responses represent a new type of structural deformation behavior in strong covalent solids. These findings may also explain the experimentally observed improvement of the ductility of boron doped
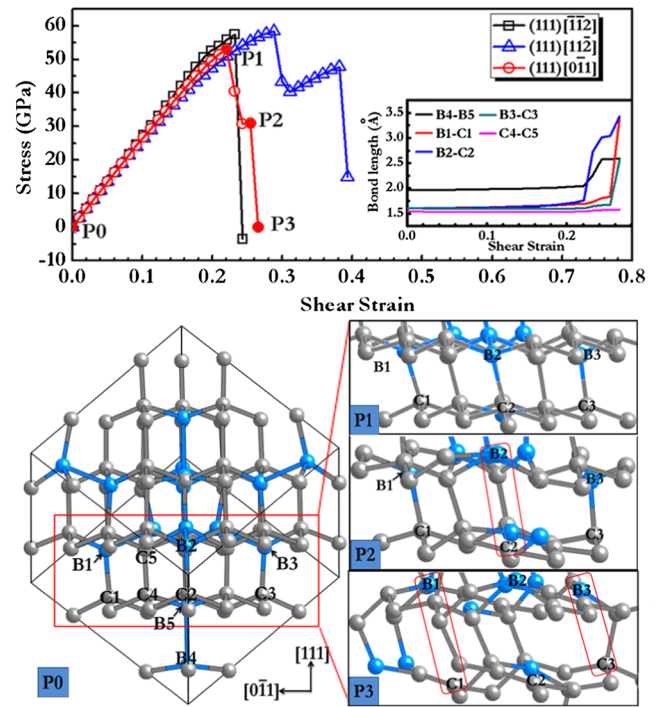

FIG. 5 (color online).   Top panel: calculated shear stress-strain relations for d-BC_3 in the (111) easy cleavage plane. Inset shows bond lengths under the $(111)[0\bar{1}1]$ shear strain. Bottom panels: structural snapshots corresponding to the filled symbols in the stress-strain plot. Local bonding structure in the red box in $P0$ is highlighted in $P1$–$P3$ to show the detailed bond deformation and breaking process.

diamond [1–3], and the sequential bond-breaking modes offer a generic mechanism to explore other strong covalent compounds with multiple bonding configurations.

In summary, we have solved the crystal structure of recently synthesized cubic BC_3 by performing a swarm structure search. In contrast to previously proposed tetragonal and orthorhombic structures, our search discovers a highly symmetric BC_3 phase in the cubic diamond structure, which becomes stable above 41.3 GPa, in good agreement with the reported synthesis pressure of 39 GPa. Simulated x-ray diffraction and Raman spectra of the predicted d-BC_3 phase are in excellent agreement with experimental data. Calculated hardness and ideal strength results demonstrate that d-BC_3 is an intrinsic superhard material, and its deformation modes under tensile and shear strains show intriguing bond elongation and sequential bond-breaking processes that lead to remarkable extended ductility and elastic response. These results represent a significant advance in understanding a distinct type of superhard material that exhibits superior ductility compared to diamond and c-BN. These new findings offer insights for exploring other complex strong covalent solids.

---

*liquan777@calypso.cn
†chen@physics.unlv.edu
‡mym@calypso.cn

[1] T. Yano, E. Popa, D. A. Tryk, K. Hashimoto, and A. Fujishima, J. Electrochem. Soc. **146**, 1081 (1999).
[2] J. Isberg, J. Hammersberg, E. Johansson, T. Wikström, D. J. Twitchen, A. J. Whitehead, S. E. Coe, and G. A. Scarsbrook, Science **297**, 1670 (2002).
[3] N. V. Novikov, J. Mater. Process. Technol. **161**, 169 (2005).
[4] E. Ekimov, V. Sidorov, E. Bauer, N. Mel'Nik, N. Curro, J. Thompson, and S. Stishov, Nature (London) **428**, 542 (2004).
[5] V. L. Solozhenko, O. O. Kurakevych, D. Andrault, Y. Le Godec, and M. Mezouar, Phys. Rev. Lett. **102**, 015506 (2009).
[6] P. Zinin, L. Ming, H. Ishii, R. Jia, T. Acosta, and E. Hellebrand, J. Appl. Phys. **111**, 114905 (2012).
[7] Z. Y. Liu, J. L. He, J. Yang, X. J. Guo, H. Sun, H.-T. Wang, E. Wu, and Y. J. Tian, Phys. Rev. B **73**, 172101 (2006).
[8] H. Liu, Q. Li, L. Zhu, and Y. M. Ma, Phys. Lett. A **375**, 771 (2011).
[9] Q. Li, H. Wang, Y. Tian, Y. Xia, T. Cui, J. He, Y. Ma, and G. Zou, J. Appl. Phys. **108**, 023507 (2010).
[10] Y. Liang, W. Zhang, J. Zhao, and L. Chen, Phys. Rev. B **80**, 113401 (2009).
[11] P. Lazar and R. Podloucky, Appl. Phys. Lett. **94**, 251904 (2009).
[12] A. S. Mikhaylushkin, X. Zhang, and A. Zunger, Phys. Rev. B **87**, 094103 (2013).
[13] Y. Wang, J. Lv, L. Zhu, and Y. Ma, Phys. Rev. B **82**, 094116 (2010).
[14] Y. Wang, J. Lv, L. Zhu, and Y. Ma, Comput. Phys. Commun. **183**, 2063 (2012). The CALYPSO code is free for academic use; please register at http://www.calypso.cn.
[15] J. Lv, Y. Wang, L. Zhu, and Y. Ma, Phys. Rev. Lett. **106**, 015503 (2011).
[16] L. Zhu, H. Wang, Y. Wang, J. Lv, Y. Ma, Q. Cui, Y. Ma, and G. Zou, Phys. Rev. Lett. **106**, 145501 (2011).
[17] Q. Li, D. Zhou, W. Zheng, Y. Ma, and C. Chen, Phys. Rev. Lett. **110**, 136403 (2013).
[18] J. P. Perdew, K. Burke, and M. Ernzerhof, Phys. Rev. Lett. **77**, 3865 (1996).
[19] G. Kresse and J. Furthmuller, Phys. Rev. B **54**, 11169 (1996).
[20] G. Kresse and D. Joubert, Phys. Rev. B **59**, 1758 (1999).
[21] A. Togo, F. Oba, and I. Tanaka, Phys. Rev. B **77**, 184101 (2008).
[22] A. Togo, F. Oba, and I. Tanaka, Phys. Rev. B **78**, 134106 (2008).
[23] P. Giannozzi, S. Baroni, N. Bonini, M. Calandra, R. Car, C. Cavazzoni, D. Ceresoli, G. L. Chiarotti, M. Cococcioni, and I. Dabo, J. Phys. Condens. Matter **21**, 395502 (2009).
[24] F. Gao, J. He, E. Wu, S. Liu, D. Yu, D. Li, S. Zhang, and Y. Tian, Phys. Rev. Lett. **91**, 015502 (2003).
[25] J. He, L. Guo, X. Guo, R. Liu, Y. Tian, H. Wang, and C. Gao, Appl. Phys. Lett. **88**, 101906 (2006).
[26] See Supplemental Material at http://link.aps.org/supplemental/10.1103/PhysRevLett.114.015502, which includes Refs. [27–43].
[27] W. L. Mao, H. K. Mao, P. J. Eng, T. P. Trainor, M. Newville, C. Kao, D. L. Heinz, J. Shu, Y. Meng, and R. J. Hemley, Science **302**, 425 (2003).
[28] S. Iijima, Nature (London) **354**, 56 (1991).
[29] W. Krätschmer, L. D. Lamb, K. Fostiropoulos, and D. R. Huffman, Nature (London) **347**, 354 (1990).
[30] K. Kikuchi, N. Nakahara, T. Wakabayashi, S. Suzuki, H. Shiromaru, Y. Miyake, K. Saito, I. Ikemoto, M. Kainosho, and Y. Achiba, Nature (London) **357**, 142 (1992).
[31] S. Nakano, M. Akaishi, T. Sasaki, and S. Yamaoka, Chem. Mater. **6**, 2246 (1994).
[32] E. Knittle, R. B. Kaner, R. Jeanloz, and M. L. Cohen, Phys. Rev. B **51**, 12149 (1995).
[33] T. Komatsu, M. Nomura, Y. Kakudate, and S. Fujiwara, J. Mater. Chem. **6**, 1799 (1996).
[34] V. L. Solozhenko, D. Andrault, G. Fiquet, M. Mezouar, and D. C. Rubie, Appl. Phys. Lett. **78**, 1385 (2001).
[35] Y. Zhao, D. W. He, L. L. Daemen, T. D. Shen, R. B. Schwarz, Y. Zhu, D. L. Bish, J. Huang, J. Zhang, G. Shen, J. Qian, and T. W. Zerda, J. Mater. Res. **17**, 3139 (2002).
[36] Y. Xu, L. Zhang, T. Cui, Y. Li, Y. Xie, W. Yu, Y. Ma, and G. Zou, Phys. Rev. B **76**, 214103 (2007).
[37] W. Utsumi and T. Yagi, Science **252**, 1542 (1991).
[38] T. Hashimoto, T. Miyoshi, and H. Ohtsuka, Phys. Rev. B **13**, 1119 (1976).
[39] V. S. Sundaram, B. Farrell, R. S. Alben, and W. D. Robertson, Phys. Rev. Lett. **31**, 1136 (1973).
[40] R. T. Howie, C. L. Guillaume, T. Scheler, A. F. Goncharov, and E. Gregoryanz, Phys. Rev. Lett. **108**, 125501 (2012).
[41] C. J. Pickard and R. J. Needs, Nat. Phys. **3**, 473 (2007).
[42] H. Liu, L. Zhu, W. Cui, and Y. Ma, J. Chem. Phys. **137**, 074501 (2012).
[43] R. T. Howie, T. Scheler, C. L. Guillaume, and E. Gregoryanz, Phys. Rev. B **86**, 214104 (2012).
[44] M. Lazzeri and F. Mauri, Phys. Rev. Lett. **90**, 036401 (2003).
[45] A. Zunger, S.-H. Wei, L. G. Ferreira, and J. E. Bernard, Phys. Rev. Lett. **65**, 353 (1990).
[46] S.-H. Wei, L. G. Ferreira, J. E. Bernard, and A. Zunger, Phys. Rev. B **42**, 9622 (1990).
[47] J. Li, K. J. Van Vliet, T. Zhu, S. Yip, and S. Suresh, Nature (London) **418**, 307 (2002).
[48] C. R. Krenn, D. Roundy, M. L. Cohen, D. C. Chrzan, and J. W. Morris, Jr., Phys. Rev. B **65**, 134111 (2002).
[49] Y. Zhang, H. Sun, and C. F. Chen, Phys. Rev. Lett. **93**, 195504 (2004).
[50] Y. Zhang, H. Sun, and C. F. Chen, Phys. Rev. Lett. **94**, 145505 (2005).
[51] Y. Zhang, H. Sun, and C. Chen, Phys. Rev. B **73**, 144115 (2006).
[52] Z. Pan, H. Sun, and C. F. Chen, Phys. Rev. Lett. **98**, 135505 (2007).
[53] Z. Pan, H. Sun, Y. Zhang, and C. F. Chen, Phys. Rev. Lett. **102**, 055503 (2009).
[54] W. Zhou, H. Sun, and C. F. Chen, Phys. Rev. Lett. **105**, 215503 (2010).